Pressure-driven evolution of upper critical field and Fermi surface reconstruction in the strong-coupling superconductor Ti_4Ir_2O

Lifen Shi,[1,2,*] Binbin Ruan,[1,*] Pengtao Yang,[1] Ningning Wang,[1,2] Pengfei Shan,[1,2] Ziyi Liu,[1] Jianping Sun,[1,2,4] Yoshiya Uwatoko,[3] Genfu Chen,[1,2,4] Zhian Ren,[1,2,†] Bosen Wang,[1,2,4,‡] and Jinguang Cheng[1,2]

[1]*Beijing National Laboratory for Condensed Matter Physics and Institute of Physics, Chinese Academy of Sciences, Beijing 100190, China*

[2]*School of Physical Sciences, University of Chinese Academy of Sciences, Beijing 100190, China*

[3]*Institute for Solid State Physics, University of Tokyo, Kashiwanoha 5-1-5, Kashiwa, Chiba 277–8581, Japan*

[4]*Songshan Lake Materials Laboratory, Dongguan, Guangdong 523808, China*

(Received 22 January 2023; revised 4 May 2023; accepted 12 May 2023; published 30 May 2023)

We report pressure-driven evolution of the superconducting transition temperature (T_c) and upper critical field B_{c2} (0) of strong-coupling superconductor Ti_4Ir_2O that possesses an unusually large B_{c2} (0) at ambient pressure (AP). Our results reveal an extremely low-pressure coefficients of T_c, i.e., $dT_c/dP \approx -0.047$ K/GPa for $P < 15$ GPa and -0.017 K/GPa for $15 < P < 50$ GPa, presumably associated with an inherent large bulk modulus of $\sim$ 252 GPa. Interestingly, we find that its B_{c2} (0) undergoes a smooth crossover at 35.6 GPa from well beyond to less than the Pauli paramagnetic limit $B_p^{BCS}(0) = 1.84\,T_c$; i.e., the $B_{c2}(0) \approx 18.2$ T $= 1.7\,B_p^{BCS}$ (0) at AP decreases to ~ 5.8 T $= 0.88\,B_p^{BCS}$ (0) at 50 GPa. The density-functional calculations predict the possible occurrence of pressure-induced Fermi surface reconstruction for the energy bands near the K point with strong spin-orbit coupling in 31–41 GPa. The present work sheds more light on this intriguing superconductor capable of resisting large external compression and strong magnetic fields.

DOI: 10.1103/PhysRevB.107.174525

I. INTRODUCTION

The upper critical field B_{c2} of type-II superconductor is a fundamental quantity closely related with the superconducting microscopic parameters including the coherence length, the superconducting gap symmetry, the superconducting coupling strength, and the pair-breaking mechanism. Usually, a large B_{c2} (0) beyond the weak-coupling BCS Pauli limit [$B_p^{BCS}(0) \approx 1.84\,T_c$] can be taken as an important indicator of unconventional Cooper pairing mechanism as exemplified in the heavy-fermion superconductors [1,2], cuprates [3], and iron-based high-T_c superconductors [4–6], as well as quasi-one-dimensional or monolayer superconductors [7–12]. Thus, the discovery of new superconducting materials with a large B_{c2} (0) value is important not only for the design of commercial superconducting magnets, but also for unveiling the underlying pairing mechanisms of unconventional superconductivity (SC) involving structural/magnetic quantum fluctuations [13–15], strange metal [16], nontrivial topological electronic states [17], enhanced spin-orbit coupling (SOC) [18,19], strong electron correlations, and multiband effects [5]. In addition to a large B_{c2} (0), a superconducting material possessing excellent mechanical properties such as strong hardness and large bulk modulus [18,19] is also desirable for applications in harsh conditions. However, most known superhard materials are usually characterized as phonon-mediated and weak-coupling SC with small B_{c2} (0) [18,19]. In this regard, it is intriguing to find new superconductors possessing both excellent mechanical properties and strong-coupling SC.

Recently, the $\eta-$carbide $-$ type Ti_4X_2O (X = Co, Rh, and Ir) [20,21], $Zr_4Rh_2O_{0.6}$ [22], and $Nb_4Rh_2C_{1-\delta}$ [23] were identified as novel superconductors with unusually large B_{c2} (0) exceeding the B_p^{BCS} (0) values and thus have attracted considerable attention. These compounds crystallize into a cubic structure with space group $Fd-3m$ (No. 227) as depicted in Fig. 1(a) for Ti_4X_2O as an example: Ti1(16c), Ti2(48f), and X(32e) atoms form a Ti_2Ni-type framework with interstitial O atoms (16d); the corner-sharing Ti1 and X tetrahedra form a "*stella quadrangular*" lattice [24]. The superconducting properties of Ti_4X_2O vary sensitively depending on the X ion, e.g., the T_c rises from 2.7, 2.8 to 5.3 K, while the B_{c2} (0) changes nonmonotonically from 7.08, 5.15 to 16.06 T for X = Co, Rh, and Ir, respectively [21]. Density of state at the Fermi level $N(E_F)$ was found to reduce monotonically from 11.22 to 9.64 and 7.50 states eV^{-1} per f.u., which is inversely proportional to the variation of T_c [21] for X = Co, Rh, and Ir, while the electron-phonon coupling constant $\lambda_{ep} \sim 0.51$–0.66 for them is comparable. To reconcile these intriguing features, other important factors such as the enhanced SOC from Co$-3d$, Rh$-4d$ to Ir$-5d$ electrons should be considered. Usually, the SOC can induce novel SC with mixed spin-singlet and -triplet superconducting state [25–27]. Indeed, among the series of Ti_4X_2O, Ti_4Ir_2O with Ir$-5d$ electrons shows the highest T_c and the largest B_{c2} (0). Theoretical calculations on the $N(E_F)$ of Ti_4Ir_2O have revealed a strong hybridization of Ti$-3d$ and Ir$-5d$ orbitals with strong SOC [20]. It has been argued that its large B_{c2} (0) should originate from a combination of

*These authors contributed equally to this work.
†renzhian@iphy.ac.cn
‡bswang@iphy.ac.cn

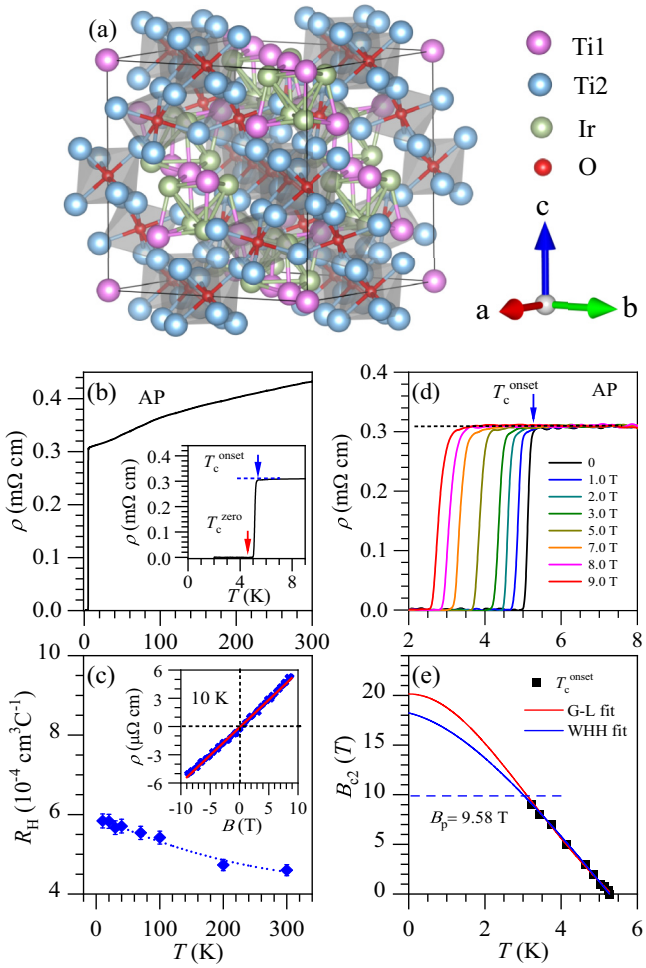

FIG. 1. (a) Crystal structure of Ti_4X_2O. (b) $\rho(T)$ of Ti_4Ir_2O at AP. Inset shows the enlarged view of the superconducting transition at low temperatures. (c) Hall coefficient R_H at various temperatures. Inset shows an example at 10 K. (d) Temperature dependence of resistivity $\rho(T)$ under various magnetic fields. (d) Upper critical fields B_{c2} vs temperature at AP and the fitting results by the Ginzburg-Landau (GL) equation and the Werthamer-Helfand-Hohenberg (WHH) model. Dashed line represents the Pauli limit.

strong-coupled SC, large SOC, and electron correlations. In experiments, the strong electron correlations were evidenced by large Wilson ratio $R_W \sim 3.9$, the Kadowaki-Woods ratio $A/\gamma^2 \approx 9 \times 10^{-6}\,\mu\Omega\,\mathrm{cm}/(\mathrm{mJ\,mol^{-1}\,K^{-1}})^2$, and Sommerfeld coefficient $\gamma = 33.74\,\mathrm{mJ\,mol^{-1}\,K^{-2}}$ [20]. Nonetheless, the role of SOC on the superconducting properties remains elusive. More studies are thus highly desirable to gain a deeper understanding of the intriguing properties of Ti_4Ir_2O.

Hydrostatic physical pressure is a clean and effective method to regulate the crystal and electronic structures of superconductors. The variations of electron correlations, electron-phonon coupling, and SOC upon compression can provide valuable information on superconducting mechanisms. Following this idea, we carried out a comprehensive high-pressure (HP) study on the strong-coupled new superconductor Ti_4Ir_2O through the measurements of x-ray diffraction and electrical transport under various pressures as well as the density-functional theory (DFT) calculations. We find an extremely low-pressure coefficient of T_c and attribute it to its strong incompressibility, i.e., large bulk modulus of 252 GPa, which suggests that Ti_4Ir_2O can be regarded as a rare example combining superior mechanical properties and strong-coupling superconducting state. With increasing pressure, the B_{c2} (0) undergoes a gradual crossover from beyond to less than B_p^{BCS} (0) at 35.6 GPa, which might be related to the Fermi surface reconstruction for the energy bands around the K point with strong SOC according to our DFT results.

II. EXPERIMENTAL METHODS

Polycrystalline Ti_4Ir_2O was synthesized by solid-state reaction method as reported elsewhere [20]. Rietveld refinements on room-temperature x-ray diffraction (XRD) pattern confirmed high-quality single phase with lattice parameter $a = 11.6194(1)$ Å. At ambient pressure (AP), electrical resistivity $\rho(T)$ and Hall resistivity $\rho_{xy}(H)$ were measured by the standard four-probe method on the Physical Property Measurement System (PPMS-9T, Quantum Design). HP resistance $R(T)$ was measured by a standard four-probe method in a commercial nonmagnetic CuBe diamond-anvil cell (DAC) of 300-μm anvil culet. A rhenium gasket was preindented to $\sim 36\,\mu$m and then a 100-μm-diameter hole was drilled by a laser drilling system. The metallic gasket was then covered with c-BN epoxy insulating layer. Ti_4Ir_2O pellet with the size of $\sim 80 \times 45 \times 12\,\mu\mathrm{m}^3$ was placed in the center of hole filled with soft KBr as the pressure-transmitting medium (PTM). Pressure was determined by the shift of the $R1$ fluorescence line of ruby below 30 GPa and the Raman spectrum of diamond up to 50 GPa. Low-temperature experiments are carried out in a ^{4}He cryostat equipped with a 9-T superconducting magnet. HP-XRD was collected at the BL15U1 station of Shanghai Synchrotron Radiation Facility (SSRF). The Au powder was mixed with Ti_4Ir_2O for pressure calibration and the 4:1 methanol-ethanol as the PTM. Lattice parameters were extracted from the XRD patterns by the GSAS software [28].

DFT calculations were carried out by using the QUANTUM ESPRESSO (QE) package [29–31]. We used the projector augmented-wave pseudopotentials with Perdew-Burke-Ernzerhof exchange-correlation density functional (PBEsol) [32] exchange-correlation functionals, as implemented in the PSLIBRARY [33]. Before self-consistent calculations of electronic structures, the atomic positions were relaxed while setting the lattice parameters to the experimental ones. The charge density, as well as the stress, were calculated by using a Monkhorst-Pack grid of 7^3 k points, while a denser grid of 21^3 k points was used to calculate the density of states (DOS) and the Fermi surfaces.

III. RESULTS AND DISCUSSION

Before performing HP studies, we first characterized the physical properties of Ti_4Ir_2O at AP. As shown in Fig. 1(b), $\rho(T)$ shows a metallic behavior with an abrupt superconducting transition at $T_c \approx 5$ K. $\rho_{xy}(B)$ measured at each temperature show linear B dependence with a positive slope [inset of Fig. 1(c)], confirming the dominant hole-type carriers. Hall coefficient $R_H = d\rho_{xy}/dB$ increases monotonously upon cooling down [Fig. 1(c)], which indicates a decrease of

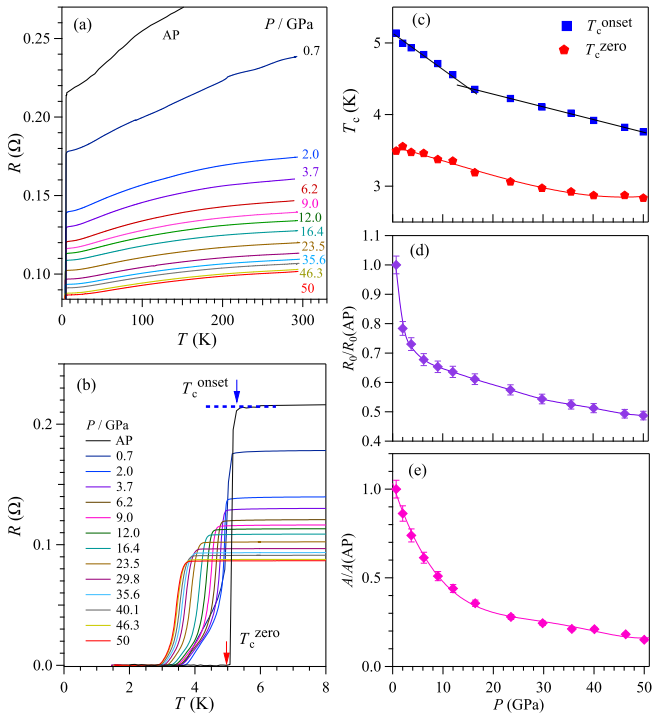

FIG. 2. (a) $R(T)$ of Ti_4Ir_2O under various pressures up to 50 GPa; (b) low-T $R(T)$; blue and red arrows indicate the T_c^{onset} and T_c^{zero}, respectively. Pressure dependence of parameters: (c) T_c^{onset} and T_c^{zero}; (d) R_0/R_0 (AP); and (e) A/A (AP).

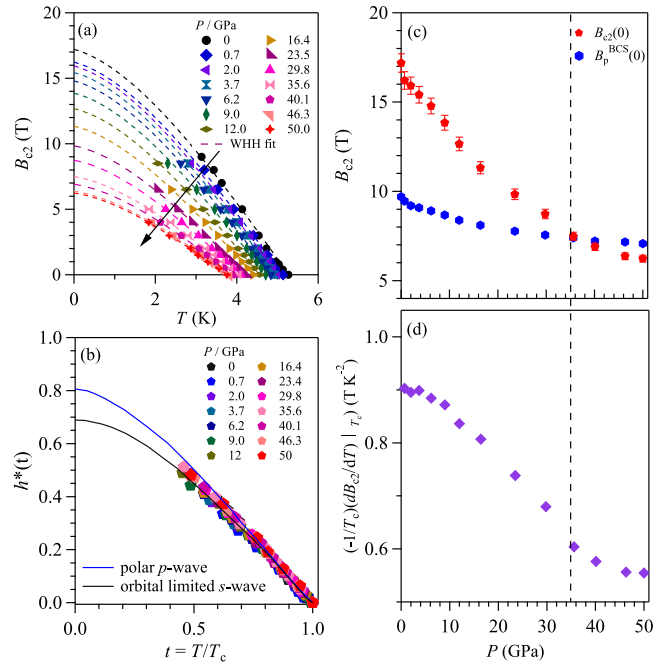

FIG. 3. (a) Temperature dependence of $B_{c2}(T)$ under various pressures. Dashed lines represent the fitting of WHH model. Black arrow represents the change trend. (b) Normalized upper critical field $h^* = B_{c2}(0)/T_c[(-dB_{c2}/dT)_{Tc}]$ vs. the reduced temperature $t = T/T_c$ by the orbital limited s-wave and the polar p-wave model ($h^* \approx 0.8$), respectively. Pressure dependence of parameters: (c) $B_{c2}(0)$ and $B_p^{BCS}(0)$ and (d) normalized upper critical field slope, $-(1/T_c)(dB_{c2}/dT)|_{Tc}$.

carrier concentration and/or an increase of carrier mobility. The superconducting transition shifts down with increasing B in Fig. 1(d). We adopted the criteria of the onset of T_c and plotted the T-dependent $B_{c2}(T)$ in Fig. 1(e). The $B_{c2}(T)$ can be fitted by using the Ginzburg-Landau (GL) equation, viz., $B_{c2}(T) = B_{c2}(0)(1-t^2)/(1+t^2)$ with $t = T/T_c$, or the Werthamer-Helfand-Hohenberg (WHH) model in a clean limit [23], viz., $B_{c2}(T) = B_{c2}(0)\,[(1-t)\text{–}C_1(1-t)^2 - C_2(1-t)^4]/0.73$ with $C_1 = 0.135$ and $C_2 = 0.134$, respectively. The extracted $B_{c2}(0) = 20.1$ and 18.2 T for the GL and WHH models are much larger than the $B_p^{BCS}(0) = 1.84$ $T_c = 9.58$ T at AP, in accordance with the published results [20,21].

To trace the normal- and superconducting-state properties of Ti_4Ir_2O under pressures, $R(T)$ was measured with DAC up to 50 GPa. As seen in Figs. 2(a) and 2(b), with increasing P, $R(T)$ decreases monotonically and the superconducting transition becomes broadened up with an obvious tail, which should be ascribed to the pressure inhomogeneity or the presence of shear stress in DAC. Both T_c^{onset} and T_c^{zero} are reduced by pressure and experience a slope change at $\sim$ 15 GPa as indicated by the intersection of two straight lines in Fig. 2(c). The pressure coefficient of T_c^{onset} is extremely low, i.e., $dT_c/dP \approx -0.047$ K/GPa for $P < 15$ GPa is further reduced to -0.017 K/GPa for $15 < P < 50$ GPa. We found that the slope change of $T_c(P)$ at $\sim$ 15 GPa correlates closely with the normal-state properties just above T_c, which are characterized by the quadratic-T coefficient of resistance. As seen in Fig. S1 [34], the $R(T)$ just above T_c can be well described by the Fermi liquid behavior, i.e., $R = R_0 + AT^2$, where the R_0 is the residual resistance and the quadratic-T coefficient A is proportional to $N(E_F)$. As can be seen in Figs. 2(d) and 2(e), both the normalized R_0/R_0(AP) and A/A(AP) tend to level off at $P > 15$ GPa, which implies that the variations of $N(E_F)$ are less effective at pressures above 15 GPa.

To investigate the pressure dependence of B_{c2} (0), the $R(T)$ of Ti_4Ir_2O were measured under different magnetic fields at each P as shown in Fig. S2 [34]. Using these data and the criteria of T_c^{onset}, the B_{c2} (0) was extracted by GL (Fig. S3) [34] and WHH models [Fig. 2(a)], respectively. The pressure dependence of obtained B_{c2} (0) based on WHH model is plotted in Fig. 3(c) together with B_p^{BCS} (0) for comparison. We can see that the B_{c2} (0) reduces from $\sim$ 18.2 T at AP to $\sim$ 5.8 T at 50 GPa and experiences a smooth crossover from well beyond to less than B_p^{BCS} (0) at 35.6 GPa.

Generally, the slope of the normalized B_{c2} (0) by T_c is closely related to Fermi velocity and the superconducting gap symmetry [35]. As shown in Fig. 3(d), the pressure dependence of $-(1/T_c)(dB_{c2}(0)/dT)|_{Tc}$ also exhibits an apparent slope change at 35.6 GPa, which coincides well with the critical pressure of the crossover $B_{c2}(0)/B_P^{BCS}(0) \approx 1$. To figure out the underlying mechanism responsible for the observed crossover, we first examined the superconducting gap symmetry by plotting the normalized upper critical field $h^* = B_{c2}(0)/T_c[(-dB_{c2}/dT)_{Tc}]$ versus the reduced temperature $t = T/T_c$ in Fig. 3(b). As can be seen, all data points collapse into one well-defined curve, which can be described by the orbital limited s-wave model but deviates from the

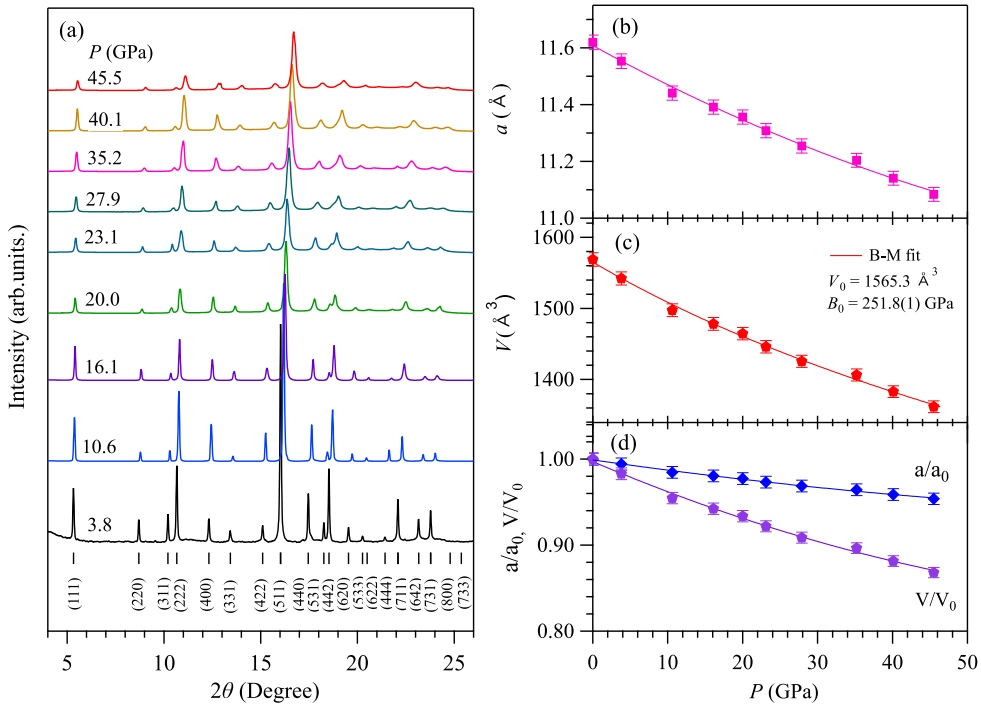

FIG. 4. (a) XRD patterns of Ti_4Ir_2O under various pressures. Pressure dependence of parameters: (b) lattice parameter a, (c) volume V, and (d) relative change a/a_0 and V/V_0. Solid lines in (c) show the Birch-Murnaghan (B-M) fitting.

polar p-wave one [36–38]. This result proves that the superconducting gap symmetry of Ti_4Ir_2O remains unchanged in the investigated pressure range. Based on these analyses, the gradual crossover of B_{c2} (0) as a function of pressure should not involve the change of superconducting pairing symmetry.

To investigate possible structural change of Ti_4Ir_2O upon compression, we measured the XRD patterns up to 45.5 GPa. As shown in Fig. 4(a), neither splitting of diffraction peaks nor new peaks was observed, confirming the absence of major structural transition in the investigated pressure range. Figures 4(b)–4(d) display the pressure dependences of a and V as well as their relative changes, a/a_0 and V/V_0, which all decrease continuously and are reduced by -4.6% for a and -13.2% for V at 45.5 GPa. Fitting of $V(P)$ to the Birch-Murnaghan equation yields a bulk modulus $B_0 = 251.8(1)$ GPa, $B' = 4$ (fixed), and $V_0 = 1565.3\,\text{Å}^3$, respectively. The obtained B_0 is much larger than the typical values of intermetallic compounds and close to the upper limit of perovskite-type oxides with a large incompressibility [39–42]. As mentioned above, most superhard and superconducting materials belong to the weak-coupling electron-phonon mediated superconductor, e.g., the B-doped diamond [43], FeB_4 [44], ZrB_{12} [45], and Mo_3C_2 [46]. In this regard, the strong-coupling superconductor Ti_4Ir_2O with excellent mechanical properties should be of special interest for practical applications.

From the above analyses, we conclude that the crossover of B_{c2} (0) cannot be ascribed to the structural transition or the change of superconducting gap symmetry but may be associated with subtle modification of electronic structures upon compression. To further substantiate this point, we performed DFT calculations on the electronic structures of Ti_4Ir_2O up to 53 GPa. The results are summarized in Fig. 5(a). For each pressure, there are five bands crossing Fermi level, consistent with the metallic nature and multiband superconducting properties of Ti_4Ir_2O [20]. Due to the presence of inherent strong SOC, a clear band splitting of Ir$-5d$ electrons occurs along the Γ-K lines. Interestingly, the band-splitting energy gap associated with SOC, ΔE_{SOC} (highlighted in the red circle) is enhanced from $\sim$ 10 meV at AP to $\sim$ 30 meV at 53 GPa. In addition, the positions of these bands also move upwards relative to the Fermi surface with increasing pressure, which results in a change from the electron- to hole-type pockets above 53 GPa. Moreover, the bands along the L-W line show stronger dispersion transiting from an approximate flatband to an electron-type pocket. These features may suggest pressure-driven Fermi surface modification. For clarification, the evolution of Fermi surfaces is presented in Fig. 5(b). As can be seen, along the Γ-K lines, the electron-like pocket at AP shrinks with pressure and its contributions to the Fermi surface varnish in the pressure range 31–41 GPa, which coincides with the critical pressure for the crossover of B_{c2} (0). In this sense, the possible presence of interband scattering in 31–41 GPa might be regarded as an important factor of large B_{c2} (0) in Ti_4Ir_2O. Similar phenomena emerge frequently in many iron-based and heavy-fermion superconductors [2,4,5,47]. Along with this, the $N(E_F)$ decreases from $8.34\,\text{eV}^{-1}$ per f.u. at AP to $5.77\,\text{eV}^{-1}$ per f.u. at 66 GPa, which is partly due to the reduced contributions of bands near K point. Our results thus demonstrate the importance of the bands along the Γ-K lines and its interband scatterings for strong-coupling superconducting states with large B_{c2} (0) at AP.

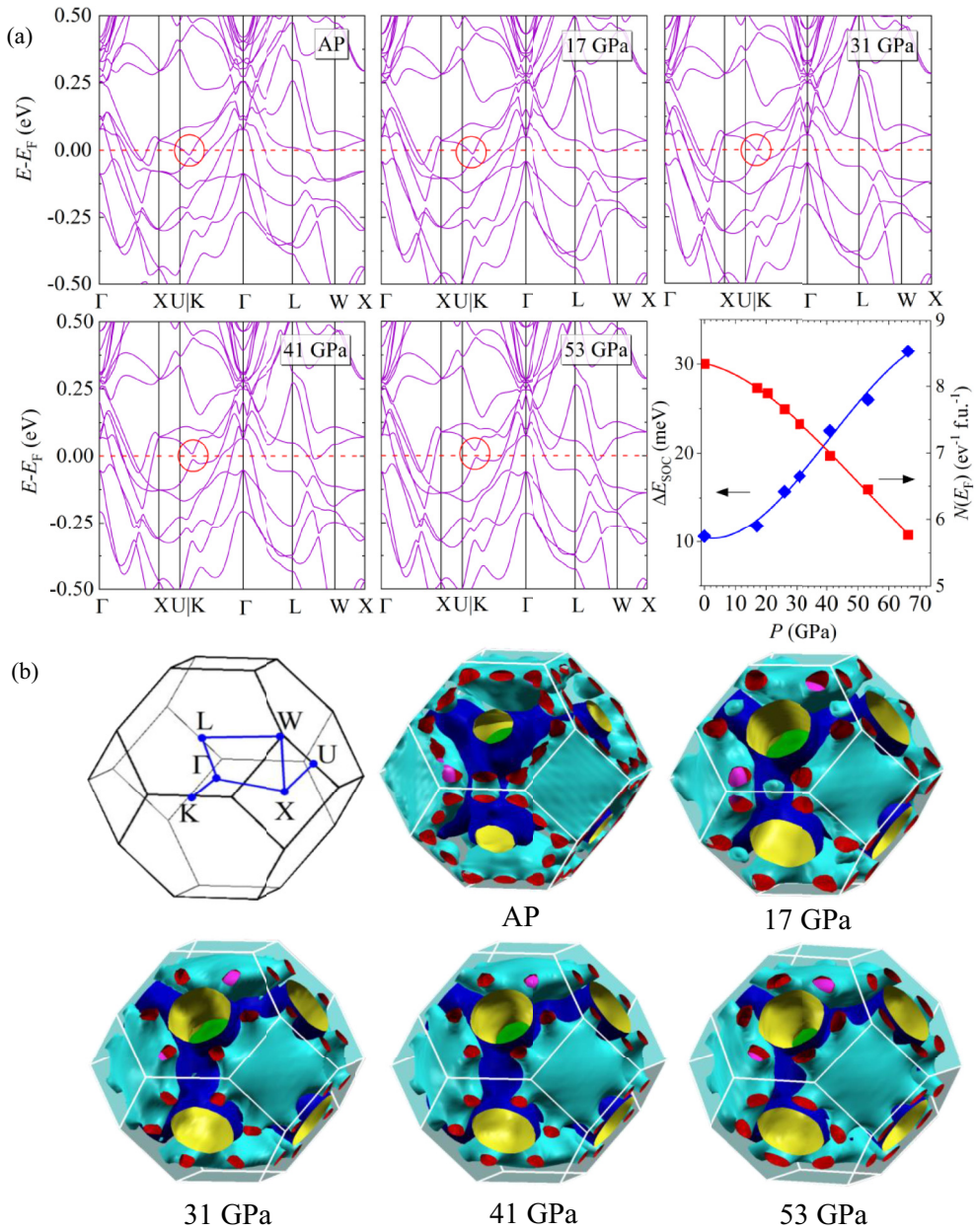

FIG. 5. (a) Electronic band structures from density-functional theory with SOC of Ti_4Ir_2O under selected pressures; P dependence of the SOC splitting energy ΔE_{SOC} and the DOS at Fermi level $N(E_F)$. Red circles emphasize the SOC splitting bands. (b) Brillouin zone and Fermi surfaces under selected pressures.

Finally, let us briefly discuss the findings of the present study. At first, we show that Ti_4Ir_2O displays an extremely low-pressure coefficient of T_c, especially at pressures above 15 GPa, i.e., $dT_c/dP \approx -0.017$ K/GPa, which is rarely seen in strong-coupling superconductors [48–50]. Such a weak pressure effect on T_c might be correlated with the low compressibility manifested by a relatively large bulk modulus of $B_0 = 252$ GPa as revealed by the HP-XRD. This discovery makes Ti_4Ir_2O a promising candidate material combining excellent mechanical properties, strong-coupling and multiband SC. At the same time, the extremely low compressibility would render quite weak modifications of lattice dynamics by pressures above 15 GPa. Then, the relative shift of SOC-related Fermi pockets around K point with respect to E_F and the changes of interband scatterings under pressures should play a dominant role in determining the evolution of superconducting coupling strength. This factor rationalizes the observed crossover of B_{c2} (0) at 35.6 GPa. Our results thus indicated that the strong-coupling SC of Ti_4Ir_2O has an intimated correlation with the SOC-derived bands around K point. We hope that this study will promote more theoretical and experimental investigations on this system for both fundamental and practical applications.

IV. CONCLUSION

In summary, we report an extremely low-pressure coefficient of T_c ($dT_c/dP \approx -0.017$ K/GPa above 15 GPa) and

large bulk modulus of $B_0 \approx 252$ GPa of Ti_4Ir_2O, demonstrating that it is a promising candidate material combining advanced mechanical properties and strong-coupling SC. We found that its B_{c2} (0) undergoes a crossover from beyond to less than the Pauli limit B_p^{BCS} (0) at 35.6 GPa, which is likely attributed to pressure-induced Fermi surface reconstruction of the SOC-derived bands around K point in Ti_4Ir_2O.

ACKNOWLEDGMENTS

This work is supported by the Beijing Natural Science Foundation (Grant No. Z190008), the National Key Research and Development Program of China (Grants No. 2018YFA0305700, No. 2018YFA0305800, No. 2021YFA1400200, No. 2018YFA0704200, and No. 2021YFA1401800), the National Natural Science Foundation of China (Grants No. 12025408, No. 11921004, No. 11834016, and No. 12074414), the Strategic Priority Research Program of CAS (Grants No. XDB25000000 and No. XDB33000000), K.C. Wong Education Foundation (Grant No. GJTD-2020-01), the Users with Excellence Program of Hefei Science Center CAS (Grant No. 2021HSC-UE008), the Youth Promotion Association of CAS (Grant No. 2018010), and the Outstanding member of Youth Promotion Association of CAS (Grant No. Y2022004). HP-XRD measurements were performed at the BL15U1 station of the Shanghai Synchrotron Radiation Facility (SSRF). This work is partially supported by the CAC station of Synergic Extreme Condition User Facility (SECUF).

[1] M. M. Altarawneh, N. Harrison, G. Li, L. Balicas, P. H. Tobash, F. Ronning, and E. D. Bauer, Phys. Rev. Lett. **108**, 066407 (2012).
[2] N. Kimura, K. Ito, H. Aoki, S. Uji, and T. Terashima, Phys. Rev. Lett. **98**, 197001 (2007).
[3] S. I. Vedeneev, A. G. M. Jansen, E. Haanappel, and P. Wyder, Phys. Rev. B **60**, 12467 (1999).
[4] H. Q. Yuan, J. Singleton, F. F. Balakirev, S. A. Baily, G. F. Chen, J. L. Luo, and N. L. Wang, Nature (London) **457**, 565 (2009).
[5] J. Jaroszynski, F. Hunte, L. Balicas, Y.-j. Jo, I. Raičević, A. Gurevich, D. C. Larbalestier, F. F. Balakirev, L. Fang, P. Cheng, Y. Jia, and H. H. Wen, Phys. Rev. B. **78**, 174523 (2008).
[6] M. Fang, J. Yang, F. F. Balakirev, Y. Kohama, J. Singleton, B. Qian, Z. Q. Mao, H. D. Wang, and H. Q. Yuan, Phys. Rev. B. **81**, 020509(R) (2010).
[7] J. F. Mercure, A. F. Bangura, X. Xu, N. Wakeham, A. Carrington, P. Walmsley, M. Greenblatt, and N. E. Hussey, Phys. Rev. Lett. **108**, 187003 (2012).
[8] J. P. Sun, Y. Y. Jiao, C. L. Yang, W. Wu, C. J. Yi, B. S. Wang, Y. G. Shi, J. L. Luo, Y. Uwatoko, and J. G. Cheng, J Phys.: Condens. Matter. **29**, 455603 (2017).
[9] K. Zhao, Q.-G. Mu, B.-B. Ruan, M.-H. Zhou, Q.-S. Yang, T. Liu, B.-J. Pan, S. Zhang, G.-F. Chen, and Z.-A. Ren, Chin. Phys. Lett. **37**, 097401 (2020).
[10] Y. Cao, J. M. Park, K. Watanabe, T. Taniguchi, and P. Jarillo-Herrero, Nature (London) **595**, 526 (2021).
[11] X. X. Xi, Z. F. Wang, W. W. Zhao, J. H. Park, K. T. Law, H. Berger, L. Forró, J. Shan, and K. F. Mak, Nat. Phys. **12**, 139 (2015).
[12] H. X. Zhang, A. Rousuli, K. Zhang, L. Luo, C. Guo, X. Cong, Z. Lin, C. Bao, H. Zhang, S. Xu, R. Feng, S. Shen, K. Zhao, W. Yao, Y. Wu, S. Ji, X. Chen, P. Tan, Q.-K. Xue, Y. Xu, W. Duan, P. Yu, and S. Zhou, Nat. Phys. **18**, 1425 (2022).
[13] P. T. Yang, Z. Y. Liu, K. Y. Chen, X. L. Liu, X. Zhang, Z. H. Yu, H. Zhang, J. P. Sun, Y. Uwatoko, X. L. Dong, K. Jiang, J. P. Hu, Y. F. Guo, B. S. Wang, and J. G. Cheng, Nat. Commun. **13**, 2975 (2022).
[14] S. S. Saxena, P. Agarwal, K. Ahilan, F. M. Grosche, R. K. W. Haselwimmer, M. J. Steiner, E. Pugh, I. R. Walker, S. R. Julian, P. Monthoux, G. G. Lonzarich, A. Huxley, I. Sheikin, D. Braithwaite, and J. Flouquet, Nature (London) **406**, 587 (2000).
[15] N. T. Huy, A. Gasparini, D. E. de Nijs, Y. Huang, J. C. Klaasse, T. Gortenmulder, A. de Visser, A. Hamann, T. Görlach, and H. von Löhneysen, Phys. Rev. Lett. **99**, 067006 (2007).
[16] J. Yuan, Q. Chen, K. Jiang, Z. Feng, Z. Lin, H. Yu, G. He, J. Zhang, X. Jiang, X. Zhang, Y. Shi, Y. Zhang, M. Qin, Z. G. Cheng, N. Tamura, Y. F. Yang, T. Xiang, J. Hu, I. Takeuchi, K. Jin, and Z. Zhao, Nature (London) **602**, 431 (2022).
[17] M. Li, Y. Liu, L. Du, X. Zhou, K. Song, R. Ji, and X. Zhao, Front. Mater. **8**, 805862 (2022).
[18] D. Rainer, G. Bergmann, and U. Eckhardt, Phys. Rev. B **8**, 5324 (1973).
[19] K. Górnicka, X. Gui, B. Wiendlocha, L. T. Nguyen, W. Xie, R. J. Cava, and T. Klimczuk, Adv. Funct. Mater. **31**, 2007960 (2020).
[20] B. B. Ruan, M. H. Zhou, Q. S. Yang, Y. D. Gu, M. W. Ma, G. F. Chen, and Z. A. Ren, Chin. Phys. Lett. **39**, 027401 (2022).
[21] K. Ma, R. Lefèvre, K. Gornicka, H. O. Jeschke, X. Zhang, Z. Guguchia, T. Klimczuk, and F. O. von Rohr, Chem. Mater. **33**, 8722 (2021).
[22] K. Ma, J. Lago, and F. O. von Rohr, J. Alloys Compd. **796**, 287 (2019).
[23] K. Ma, K. Gornicka, R. Lefèvre, Y. Yang, H. M. Rønnow, H. O. Jeschke, T. Klimczuk, and F. O. von Rohr, ACS Materials Au **1**, 55 (2021).
[24] T. Waki, S. Terazawa, T. Yamazaki, Y. Tabata, K. Sato, A. Kondo, K. Kindo, M. Yokoyama, Y. Takahashi, and H. Nakamura, EPL **94**, 37004 (2011).
[25] L. Liu, K. Okazaki, T. Yoshida, H. Suzuki, M. Horio, L. C. C. Ambolode, J. Xu, S. Ideta, M. Hashimoto, D. H. Lu, Z. X. Shen, Y. Ota, S. Shin, M. Nakajima, S. Ishida, K. Kihou, C. H. Lee, A. Iyo, H. Eisaki, T. Mikami, T. Kakeshita, Y. Yamakawa, H. Kontani, S. Uchida, and A. Fujimori, Phys. Rev. B **95**, 104504 (2017).
[26] T. Shang, S. K. Ghosh, M. Smidman, D. J. Gawryluk, C. Baines, A. Wang, W. Xie, Y. Chen, M. O. Ajeesh, M. Nicklas, E. Pomjakushina, M. Medarde, M. Shi, J. F. Annett, H. Yuan, J. Quintanilla, and T. Shiroka, npj Quantum Mater. **7**, 35 (2022).
[27] I. Bonalde, W. Bramer-Escamilla, and E. Bauer, Phys. Rev. Lett. **94**, 207002 (2005).
[28] B. H. Toby, J. Appl. Crystallogr. **34**, 210 (2001).

[29] P. Giannozzi, S. Baroni, N. Bonini, M. Calandra, R. Car, C. Cavazzoni, D. Ceresoli, G. L. Chiarotti, M. Cococcioni, I. Dabo, A. Dal Corso, S. de Gironcoli, S. Fabris, G. Fratesi, R. Gebauer, U. Gerstmann, C. Gougoussis, A. Kokalj, M. Lazzeri, L. Martin-Samos, N. Marzari, F. Mauri, R. Mazzarello, S. Paolini, A. Pasquarello, L. Paulatto, C. Sbraccia, S. Scandolo, G. Sclauzero, A. P. Seitsonen, A. Smogunov, P. Umari, and R. M. Wentzcovitch, J. Phys.: Condens. Matter. **21**, 395502 (2009).

[30] P. Giannozzi, O. Andreussi, T. Brumme, O. Bunau, M. Buongiorno Nardelli, M. Calandra, R. Car, C. Cavazzoni, D. Ceresoli, M. Cococcioni, N. Colonna, I. Carnimeo, A. Dal Corso, S. de Gironcoli, P. Delugas, R. A. DiStasio, Jr., A. Ferretti, A. Floris, G. Fratesi, G. Fugallo, R. Gebauer, U. Gerstmann, F. Giustino, T. Gorni, J. Jia, M. Kawamura, H. Y. Ko, A. Kokalj, E. Kucukbenli, M. Lazzeri, M. Marsili, N. Marzari, F. Mauri, N. L. Nguyen, H. V. Nguyen, A. Otero-de-la-Roza, L. Paulatto, S. Ponce, D. Rocca, R. Sabatini, B. Santra, M. Schlipf, A. P. Seitsonen, A. Smogunov, I. Timrov, T. Thonhauser, P. Umari, N. Vast, X. Wu, and S. Baroni, J. Phys.: Condens. Matter **29**, 465901 (2017).

[31] P. Giannozzi, O. Baseggio, P. Bonfa, D. Brunato, R. Car, I. Carnimeo, C. Cavazzoni, S. de Gironcoli, P. Delugas, F. Ferrari Ruffino, A. Ferretti, N. Marzari, I. Timrov, A. Urru, and S. Baroni, J Chem. Phys. **152**, 154105 (2020).

[32] J. P. Perdew, A. Ruzsinszky, G. I. Csonka, O. A. Vydrov, G. E. Scuseria, L. A. Constantin, X. Zhou, and K. Burke, Phys. Rev. Lett. **100**, 136406 (2008).

[33] A. Dal Corso, Comput. Mater. **95**, 337 (2014).

[34] See Supplemental Material at http://link.aps.org/supplemental/10.1103/PhysRevB.107.174525 for the temperature dependence of normal/superconducting parameters of Ti_4Ir_2O.

[35] V. G. Kogan and R. Prozorov, Rep. Prog. Phys. **75**, 114502 (2012).

[36] N. R. Werthamer, E. Helfand, and P. C. Hohenberg, Phys. Rev. **147**, 295 (1966).

[37] K. Scharnberg and R. A. Klemm, Phys. Rev. B **22**, 5233 (1980).

[38] K. Kirshenbaum, P. S. Syers, A. P. Hope, N. P. Butch, J. R. Jeffries, S. T. Weir, J. J. Hamlin, M. B. Maple, Y. K. Vohra, and J. Paglione, Phys. Rev. Lett. **111**, 087001 (2013).

[39] Y. Ma and R. Aksoy, Solid. State. Commun. **142**, 376 (2007).

[40] Y. Ma, J. Liu, C. Gao, W. N. Mei, A. D. White, and J. Rasty, Appl. Phys. Lett. **88**, 191903 (2006).

[41] D. Valim, A. G. S. Filho, P. T. C. Freire, S. B. Fagan, A. P. Ayala, J. M. Filho, A. F. L. Almeida, P. B. A. Fechine, A. S. B. Sombra, J. S. Olsen, and L. Gerward, Phys. Rev. B **70**, 132103 (2004).

[42] A. S. Verma and A. Kumar, J. Alloys Compd. **541**, 210 (2012).

[43] V. A. Sidorov, E. A. Ekimov, S. M. Stishov, E. D. Bauer, and J. D. Thompson, Phys. Rev. B **71**, 060502(R) (2005).

[44] H. Gou, N. Dubrovinskaia, E. Bykova, A. A. Tsirlin, D. Kasinathan, W. Schnelle, A. Richter, M. Merlini, M. Hanfland, A. M. Abakumov, D. Batuk, G. Van Tendeloo, Y. Nakajima, A. N. Kolmogorov, and L. Dubrovinsky, Phys. Rev. Lett. **111**, 157002 (2013).

[45] T. Ma, H. Li, X. Zheng, S. Wang, X. Wang, H. Zhao, S. Han, J. Liu, R. Zhang, P. Zhu, Y. Long, J. Cheng, Y. Ma, Y. Zhao, C. Jin, and X. Yu, Adv. Mater. **29**, 1604003 (2017).

[46] Y. Ge, S. Ma, K. Bao, Q. Tao, X. Zhao, X. Feng, L. Li, B. Liu, P. Zhu, and T. Cui, Inorg. Chem. Front. **6**, 1282 (2019).

[47] S. Khim, B. Lee, J. W. Kim, E. S. Choi, G. R. Stewart, and K. H. Kim, Phys. Rev. B **84**, 104502 (2011).

[48] K. Arii, K. Igawa, H. Takahashi, M. Imai, M. Akaishi, and I. Shirotani, J Phys. Conf. Ser. **121**, 052014 (2008).

[49] L. Shi, P. Yang, T. Wang, P. Shan, Z. Liu, S. Xu, K. Chen, N. Wang, L. Zhou, Y. Long, J. Sun, G. Mu, Y. Uwatoko, B. Wang, and J. Cheng, Phys. Rev. B **105**, 214529 (2022).

[50] I. Shirotani, K. Ohno, C. Sekine, T. Yagi, T. Kawakami, T. Nakanishi, H. Takahashi, J. Tang, A. Matsushita, and T. Matsumoto, Physica B **281**, 1021 (2000).